UNUSUAL PEGMATOID CRYSTALLISATIONS IN A NEPHELINITE PLUG, NEAR ROUND LAGOON, EASTERN CENTRAL PLATEAU, TASMANIA

by F. L. Sutherland, B. J. Barron, R. E. Pogson, J. L. Everard, S. M. Forsyth and J. D. Hollis

(with five text-figures, two plates and six tables)

Sutherland, F.L., Barron, B.J., Pogson, R.E., Everard, J.L., Forsyth, S.M. & Hollis, J.D. 2008 (28:xi): Unusual pegmatoid crystallisations in a nephelinite plug, near Round Lagoon, eastern Central Plateau, Tasmania. *Papers and Proceedings of the Royal Society of Tasmania* 142(2): 23–38. https://doi.org/10.26749/rstpp.142.2.23 ISSN 0080-4703. Geoscience, Australian Museum, 6 College Street, Sydney, New South Wales 2010, Australia (FLS*, REP); 7 Fairview Avenue, St Ives, Sydney, New South Wales 2075, Australia (BJB); Mineral Resources Tasmania, PO Box 56, Rosny Park, Tasmania 7018, Australia (JLE, SMF); "Shenley", 33 Park Street, Trentham, Victoria 3458, Australia (JDH). *Author for correspondence. Email: Lin.Sutherland@austmus.gov.au

Pegmatoids in a Late Oligocene olivine nephelinite plug near Round Lagoon form a complex low-pressure fractionation suite. The host nephelinite contains meta-peridotite and meta-wehrlite mantle xenoliths and its composition (Mg# 0.63) may reflect both mantle and then limited low-pressure fractionation. The pegmatoids range from ultramafic through mafic to feldspathic assemblages in a progressive, but discontinuous, fractionation sequence (wehrlite → olivine clinopyroxenite → sodalite ijolite, ijolite, nepheline syenite → alkali syenite). Within this sequence, olivine and clinopyroxene compositions decrease in Mg content, while clinopyroxene becomes increasingly Na- and Fe-rich to produce late stage aegirine-augite and aegirine. Nepheline is prominent in the sequence and crystallised over a wide temperature range from 1000° to <500°C. The presence of sodalite suggests volatile Cl-rich fluxing. Mg-rich spinel crystallised in early assemblages, distinct from Fe- and Ti-rich oxides of the magnetite-ulvospinel series in later assemblages. The Round Lagoon low-pressure pegmatoids developed by fractionation in a narrow, vertical feeder rather than in broad lava ponds such as those noted in nephelinite flows at Inverell, New South Wales, and at La Madera, Argentina.

Key Words: olivine nephelinite, fractionation, pegmatoids, feldspathoids, xenoliths, mantle, Tasmania.

INTRODUCTION

A diverse assemblage of mantle and crustal xenoliths and coarse-grained cognate feldspathoidal and feldspathic crystallisations has been briefly reported from an olivine nephelinite plug, on the eastern Central Plateau in Tasmania (Sutherland & Hollis 1982, Sutherland 1989, Sutherland *et al.* 1989, Everard 2001). The site lies 0.7 km east of Round Lagoon and 7 km north of Lake Sorell (Grid AMG 517600mE, 5348400mN, or 147°13.7'E, 42°00.9'S, datum AGD 66). The plug is a prominent, strongly east–west-jointed feature about 250 m across, which penetrates the eroded edge of the Jurassic dolerite sill, here about 300 m thick, which forms the Great Western Tiers. It extends from 960–1030 m asl, with its greatest exposure on the down slope side. Brecciated and altered dolerite is visible against the north side of the plug, suggesting intrusive emplacement of the nephelinite, but scree obscures the contact elsewhere. This olivine nephelinite plug was analysed and dated by the K-Ar method as Late Oligocene in age (24.9±0.2 Ma; Sutherland 1989). It is one of many basaltic plug and flow remnants mapped on the Interlaken 1:50 000 geological map sheet (Forsyth 1989). These lie west of the Tiers escarpment, formed by erosional retreat inland from the Tiers lineament that bounds the Midlands rift valley to the east (Direen & Leaman 1997). The lithospheric mantle below this region lies at a depth of about 30 km (Rawlinson *et al.* 2001).

The xenolithic and coarse cognate assemblages here form one of the most varied, and best preserved, inclusion suites in Tasmania. As well as containing fragments from the Jurassic dolerite and underlying Permian sandstones and shales, ultramafic mantle xenoliths, some cumulate-textured ultramafic to mafic pyroxenites, disaggregated xenocrysts, and coarse pegmatoidal feldspathoidal and feldspathic crystallisations also occur. The mantle xenoliths are dominated by spinel meta-lherzolite, mostly medium-grained, but finer grained types and recrystallised, partly glassy variants occur. Some olivine grains within them, up to 50 mm across, approach gem quality, but are mostly fractured. Some coarse spinel meta-lherzolites and pyroxenites exhibit lamellar exsolution of clinopyroxene in orthopyroxene. Mantle xenoliths reach up to 210 mm across. One has a composite structure (fig. 1), in which spinel meta-lherzolite is disrupted by cumulate crystallisations of transitional wehrlite (~40% olivine, 60% clinopyroxene) showing a cavity-like texture which have finer grained margins of clinopyroxenite (~olivine 5%, clinopyroxene 95%) against the host meta-lherzolite.

Abundant coarse-grained pegmatoids in the host nephelinite which have feldspathoidal and syenitic assemblages are the focus of the current investigation. One long pegmatoid vein traverses the plug, but most pegmatoids

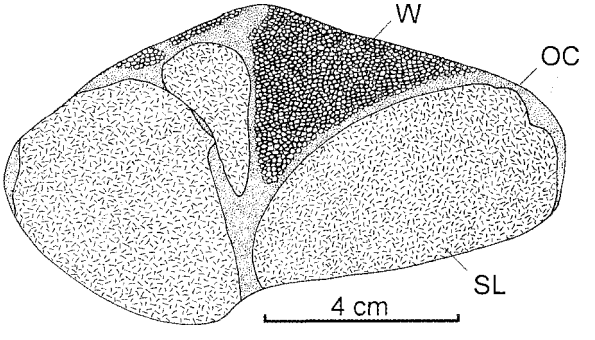

FIG. 1 — Composite mantle xenolith, showing spinel lherzolite (SL), intruded by finer grained margins of cumulate olivine clinopyroxenite (OC) and coarse cumulate wehrlite (W). Sketch by J.D. Hollis, redrawn by R.T. Springthorpe.

form discrete, subangular bodies up to a few cm across. Some rounded bodies contain internal radial growths and represent cavity fillings. Most, however, show abrupt, irregular contacts with the host. Such abundant feldspathoidal pegmatoids are rarely described from olivine nephelinites (London 2008). A single nepheline-sodalite-syenite pegmatoid from Boat Harbour, NW Tasmania (Sutherland *et al.* 1996), forms an isolated example. Pegmatoidal developments in nephelinite near Inverell, New South Wales (Wilkinson 1977), are not as mineralogically diverse as those at Round Lagoon. Abundant pegmatitic dykes occur in melanephelinite from Córdoba, Argentina (Galliski *et al.* 2004), but these are injections into a flow and differ in mineralogy to Round Lagoon pegmatoids. Pegmatoids and their low-pressure fractionation trends within olivine-melilite-nephelinite flows in Hawaii (Wilkinson & Stolz 1983) and western Bohemia (Ulrych *et al.* 2000) differ in that their assemblages include melilite. Alkali pyroxenite and ijolite materials in a nephelinite centre from Bohemia that were originally thought to be endogenous are now considered to represent a separate, deep-seated nephelinitic crystallisation (Ulrych *et al.* 2005).

This present paper documents the unusual Round Lagoon xenolith and pegmatoidal mineral assemblages, particularly the late-stage assemblages. The results are then used to evaluate the pegmatoidal assemblages in terms of fractionation trends described from nephelinites elsewhere and also compare the high-pressure ultramafic xenoliths with other Tasmanian and eastern Australian mantle suites. The term pegmatoid is preferred here over the term pegmatite, which includes much coarser assemblages associated with larger intrusive masses of alkaline and silicic rocks (London 2008).

MATERIALS AND ANALYTICAL METHODS

Thin sections and polished thin sections were prepared from samples housed in the Australian Museum collections. The study suite with sample numbers is listed in table 1. Two electron microprobe (EMP) facilities were used for mineral analyses. Analyses made on automated ETEC microprobe at Macquarie University, North Ryde, used natural standards, Bence-Albee matrix corrections, a 15 kV accelerating voltage and a sample current of 20 nA (B.J. Barron, analyst). Supplementary analyses under similar settings employed a combined wave length energy dispersive system at the Electron Microscope Unit, University of Sydney, with wave length spectrometers used to improve detection limits on key elements such as Na and K (D.F. Hendry, analyst). These methods gave precisions better than ±1 relative % for elements above 10 wt.% as oxides, ±5% for elements between 1–10 wt.% as oxides and ±10% for elements below 1 wt.%

TABLE 1
Samples studied from Round Lagoon nephelinite plug

Sample	Nature	Examination[1]	Designation[2]	Origin
RL1	Peridotite	TS, OM, PM	Spl-wehrlite	Cumulate
RL1A	Pyroxenite	TS, OM, PM	Ol-ne-clinopyroxenite	Cumulate
	Foid-syenitoid		Ijolite[3,4]	Late-stage
RL2	Peridotite	TS,OM	Spl- wehrlite	Cumulate
RL2A	Foid-syenitoid	TS,OM, EMP, PM	Ijolite[3]	Late-stage
RL3	Foidolite	TS,OM, EMP, PM	Sdl-ijolite[4]	Late-stage
RL3A	Nephelinite host	TS,OM, EMP	Ol-nephelinite[3]	Eruptive
RL3B	Pyroxenite	TS,OM	Ol-ne-clinopyroxenite	Cumulate
RL4	Foidolite	TS,OM	Ijolite[3]	Late-stage
RL5	Pyroxenite	TS,OM	Ol-ne-clinopyroxenite	Cumulate
RL6	Foid-syenitoid	TS,OM, EMP, PM	Ne-syenite[3]	Late-stage
RL6A	Peridotite	TS,OM, EMP, PM	Spl-wherlite	Meta-mantle
RL7	Pyroxenite	TS,OM	Spl-ol-clinopyroxenite	Meta-mantle
RL7A	Foid-syenitoid	TS,OM	Ne-syenite[3]	Late-stage
RL8	Peridotite	TS,OM, EMP, PM	Spl-wehrlite[4]	Cumulate
RL9	Peridotite	TS,OM, EMP, PM	Spl-lherzolite	Meta-mantle
RL10	Pyroxenite	TS,OM	Ol-clinopyroxenite	Cumulate
RL11	Foid-syenitoid	TS,OM	Ne-syenite	Late-stage
RL12	Foid-syenitoid	TS,OM,	Ne-syenite	Late-stage
RL13	Pyroxenite	TS,OM	Spl-clinopyroxenite	Meta-mantle
RL14	Pyroxenite	TS,OM	Spl-ol-websterite	Meta-mantle
RL15	Microsyenitoid	TS,OM, EMP, PM	Alkali syenite[3,4]	Late-stage
RL16	Pyroxenite	TS,OM	Spl-websterite	Meta-mantle
RL17	Peridotite	TS,OM	Olivine megacryst	Meta-mantle
RL18	Peridotite	TS,OM	Spl-lherzolite	Meta-mantle
RL19	Pyroxenite	TS,OM, EMP, PM	Ol-clinopyroxenite	Cumulate

[1] TS, thin/polished section; OM, optical microscopy; EMP, electron microprobe; PM, photomicrograph.
[2] Spl, spinel. Ol, olivine. Ne, nepheline. Sdl, sodalite.
[3] Afd, alkali feldspar. [4] Amp, amphibole.

as oxides. Comparative analyses from the two instruments mostly agreed within ±2% for oxides above 5 wt.%, within ±8% for oxides between 1–4 wt.% and ±30% for oxides below 1 wt.%. A semi-quantitative Energy Dispersive X-ray Spectrometer (Oxford Instruments Link Isis 200) at the Australian Museum, Sydney (R.E. Pogson, analyst), was used to determine the Cl content of sodalite. Photomicrographs of sections were taken using a Leica DMLP petrographic microscope, with a digital image capture systems, at the Australian Museum (pls 1, 2).

Representative analyses selected from the wider EMP data set are listed for the essential petrological assemblages in tables 2–5. The geochemical data were plotted on triangular plots and discrimination diagrams, using Geo Plot (Zhou & Li 2006). Mineral nomenclature follows International Mineralogical Association guidelines. End members for olivine are based on Deer *et al.* (1982). Pyroxene names are based on Morimoto (1988) and the computer program of Cebeira (1990). Amphibole names are based on Leake *et al.* (1997) and the computer program of Yavuz (1996). Rock names follow general recommendations in Le Maitre (2002) and for Australian intraplate volcanic rocks those in Johnson (1989). Normative mineral abbreviations follow those in Hutchison (1974), while symbols for rock-forming minerals follow Kretz (1983).

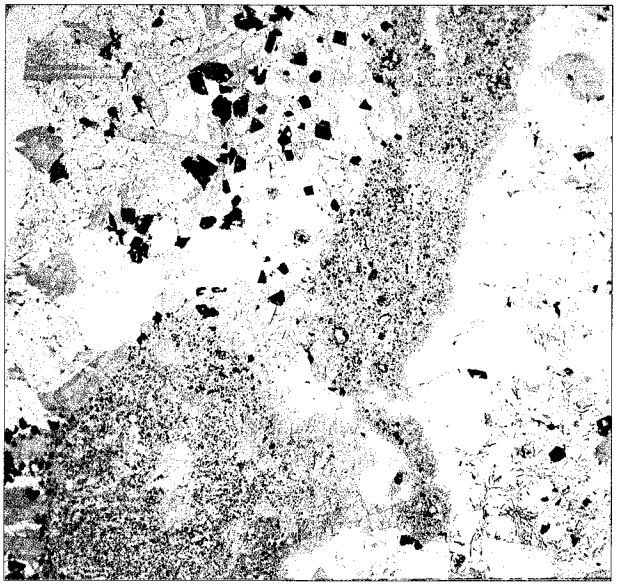

PLATE 1
Photomicrograph of olivine clinopyroxenite (bottom left) and surrounding sodalite-ijolite (right) and ijolite (top left) crystallisations in host olivine nephelinite (centre). Field of view 23 mm wide X 22 mm high. R.E. Pogson photograph.

PETROGRAPHIC RESULTS

Host nephelinite

The nephelinite contains olivine and clinopyroxene microphenocrysts up to 2 mm across in a groundmass of granular olivine, prismatic clinopyroxene, granular to subhedral equant opaque oxide grains and interstitial and partly sub-ophitic to poikilitic nepheline and alkali feldspar. Acicular apatite and small ragged flakes of dark mica are accessories. Mineral analyses (table 2) show the olivine is forsterite (fo_{72-74}), partly corroded and altered to "iddingsite". Clinopyroxene is zoned titaniferous augite-diopside (en_{41-49} $di_{40-49}fs_{10-11}$; TiO_2 2–3 wt.%) with simple to multiple twinning and partially resorbed cores in phenocrysts. Opaque oxide is magnetite-ulvospinel, which forms sporadic clusters. Nepheline is sodic ($ne_{80-81}kls_{14-15}qtz_{2-3}$); alkali feldspar is zoned from anorthoclase to sanidine ($or_{52}ab_{47}an_1$). Although overlapping, the crystallisation sequence is: olivine, clinopyroxene, ulvospinel, apatite, nepheline, alkali feldspar and zeolites.

Ultramafic cumulates

These comprise wehrlites and olivine-clinopyroxenites. The wehrlites (RL1, 2, 8; table 2; pl. 2A) contain up to 85% olivine ($fo_{90-91}fa_{9-10}$) as coarse, granular grains up to 5 mm across and as smaller inclusions in branching domains of microgranular pale green Cr-bearing augite ($en_{54-55}wo_{40-42}fs_4$; Cr_2O_3 2.2–2.5 wt.%). Accessory interstitial yellow-brown Cr-bearing spinel ($spl_{82-83}chr_{13-14}usp_2mag_{1-2}hc_1$) exhibits opaque reaction rims. Residual, branching networks and veinlets through the assemblage are composed of glassy, low relief material that contains rare phlogopite grains (Mg # 0.87), alkali feldspar, saponitic clays and other alteration products.

The olivine-clinopyroxenites (RL1A, 3B, 5, 10, 19; table 2; pl. 2B) contain intergrown crystals of Ti- and Al- bearing diopside ($wo_{51-57}en_{37-38}fs_{10-12}$; Al_2O_3 5.2–5.6 wt.%, TiO_2 2.3–2.8 wt.%), commonly up to 8 mm across or more in some cases. They include small grains of olivine (fo_{73}). Interstitial and vein-like intergrowths consist of sodic nepheline ($ne_{76-77}kls_{13-15}qtz_{10}$) and accessory alkali feldspar, ulvospinel, apatite and rare brown mica. These may form along zones of alteration in diopside. In contact with the host nephelinite, the diopside has euhedral overgrowths which lack inclusions. Rare, composite diopside aggregates show crystal growth radiating out from a nucleus of sodalite, alkali feldspar and poikilitic nepheline that encloses small olivine grains.

A notable composite pegmatoid in the host nephelinite (RL1A) contains a nepheline-olivine-bearing clinopyroxenite core within flanking ijolite and nepheline syenite pegmatoid. This illustrates a localised fractionation process within crystallising nephelinite (pl. 1).

Feldspathoid-rich pegmatoids

These foidolites range from sodalite- and nepheline-rich assemblages to nepheline-rich assemblages containing minor alkali feldspar. Typical sodalite- ($sdl_{93}k\text{-}sdl_7$) and nepheline ($ne_{67-68}kls_{29-30}qtz_3$)-rich examples (RL3, table 3, pl. 2C) contain about 50% interstitial feldspathoids (nepheline slightly exceeds sodalite) and 50% stumpy subhedral to euhedral pale yellow diopside ($wo_{46-49}en_{33-43}fs_{9-19}$), partially grading to pinkish Ti-bearing (TiO_2 2 wt.%) and dark blue-green sodic pyroxene on its rims and in adjacent grains ($acm_{53-57}wo_{17-21}en_{10-15}fs_{8-11}jd_2$). The diopside contains small inclusions of olivine (fo_{65-66}), accessory ulvospinel and aegirine-augite.

Nepheline- and alkali feldspar-rich assemblages (RL 1A, 2A, 4, 6, 11, 12; table 3, pl. 2E) contain nepheline ($ne_{82-83}kls_{15-16}qtz_2$) as oriented narrow hexagonal prismatic crystals in coarser anhedral anorthoclase ($ab_{59-61}or_{33-35}an_6$) and associated domain-zoned, anhedral pale purple Ti- and Al-bearing diopside ($wo_{50-52}en_{36-41}fs_{9-13}$; TiO_2 2–4 wt.%,

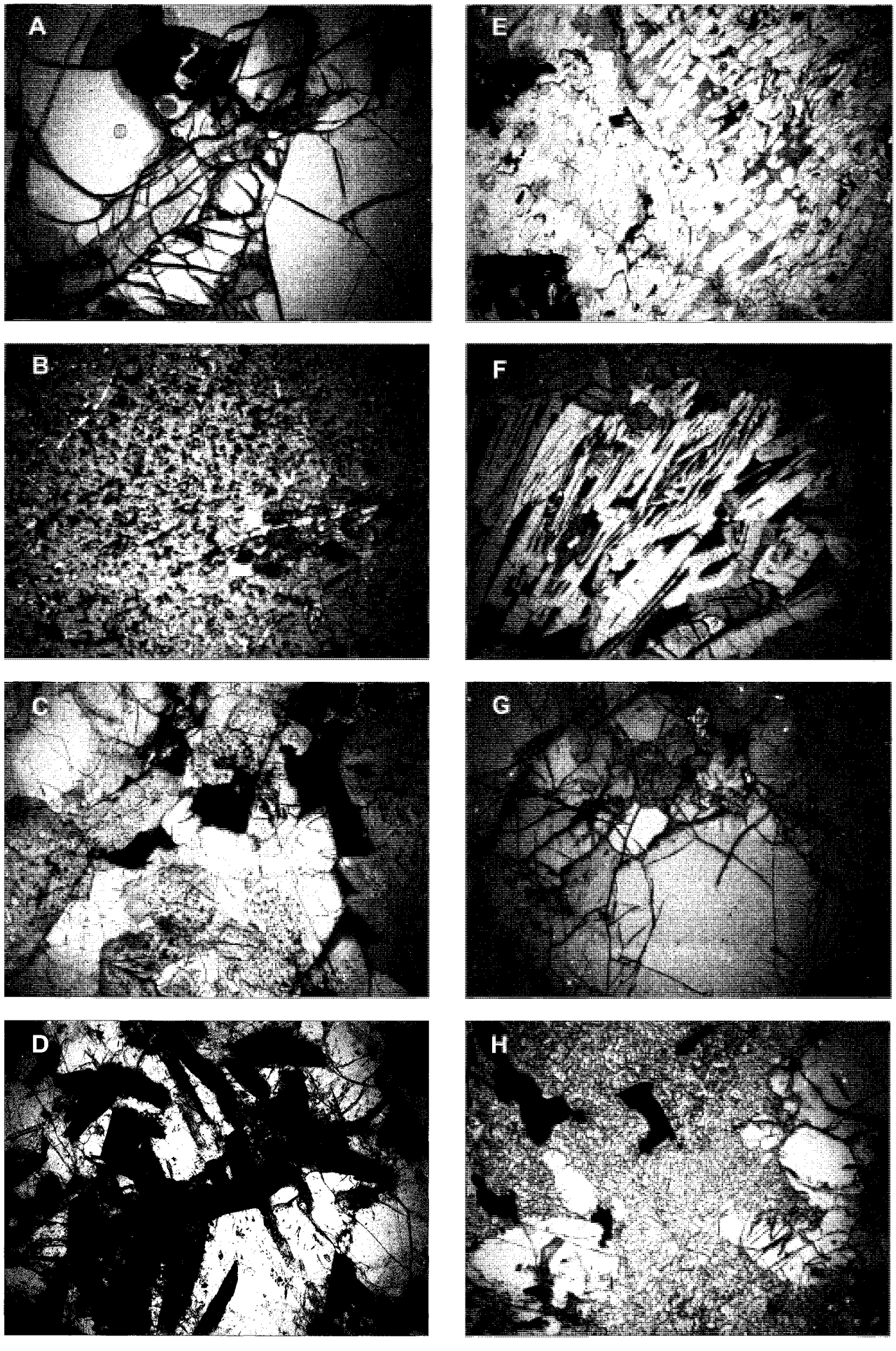
A
B
C
D
E
F
G
H

TABLE 2
Representative analyses host nephelinite and ultramafic cumulates

Analysis wt.%	Ol-nephelinite (RL3A)[1]			Wehrlite (RL8)[2]				Olv-clinopyroxenite (RL19)[3]		
Mineral	Ol	Cpx	Ne	Ol	Cpx	Spl	Clay	Cpx	Ol	Ne
SiO_2	38.62	48.95	44.33	40.82	54.88	0.59	38.12	49.03	38.35	47.48
TiO_2		2.42	0.16			0.14		2.33	0.04	0.06
Al_2O_3		5.14	32.64			53.69	15.19	5.34		31.67
Cr_2O_3		0.24			2.55	13.51	0.10	0.29		
FeO	20.39	6.04	0.85	8.74	2.66	9.18	0.29	4.98	24.32	0.76
Fe_2O_3						1.69		1.20		
MnO	0.27				0.17		0.11	0.12	0.77	0.09
MgO	40.14	13.69		49.57	18.39	21.01	25.88	12.67	36.62	0.26
CaO	0.32	22.07	0.88	0.13	18.73		0.71	24.18	0.26	0.32
Na_2O		0.68	16.48		1.26			0.41		15.32
K_2O			4.15					0.05		3.86
Total	99.74	99.23	99.49	99.26	99.11	99.81	80.40	100.50	100.36	99.82
Cations (No. O)	4	6	32	4	6	32	20	6	4	32
Si^{4+}	0.999	1.826	8.500	1.002	1.998	0.124	5.336	1.814	1.005	8.945
Ti^{4+}		0.068	0.023			0.021		0.065	0.001	0.009
Al^{3+}		0.226	7.379			13.215	2.506	0.233		7.035
Cr^{3+}		0.007			0.073	2.231	0.011	0.009		
Fe^{2+}	0.441	0.152	0.136	0.179	0.081	1.603	0.034	0.154	0.533	0.120
Fe^{3+}		0.036				0.2648		0.033		
Mn^{2+}	0.006				0.005		0.013	0.004	1.431	0.014
Mg^{2+}	1.547	0.761		1.813	1.023		5.399	0.699	0.007	0.073
Ca^{2+}	0.009	0.882	0.180	0.003	0.730	6.566	0.106	0.958		0.065
Na^{1+}		0.049	6.126		0.089			0.029		5.598
K^{1+}			1.015					0.002		0.928
Sum	3.001	4.007	23.358	2.998	4.001	24.098	12.405	4.000	2.994	22.790
Cation ratio (%)										
Mg	77.5	41.5		90.8	55.8	61.3	97.5	37.8	73.0	
Fe	22.1	10.3		9.0	4.4	17.7	0.6	10.3	27.0	
Cr						21.0				
Ca	0.4	48.2	2.46	0.2	39.8		1.9	51.9		0.9
Na			83.7							85.0
K			13.9							14.1

[1] **RL3A** Ol: Forsterite ($fo_{78}fa_{22}$); Cpx: Diopside ($wo_{48}en_{42}fs_{10}$); Ne: Nepheline ($ne_{80}kls_{14}qtz_6$).
[2] **RL8** Ol: Forsterite ($fo_{91}fa_9$); Cpx: Augite ($en_{55}wo_{40}fs_5$); Spl: Cr-rich spinel ($sp_{82}chr_{14}usp_2mag_2hc_1$);
[3] **RL19** Cpx: Diopside ($wo_{52}en_{38}fs_{10}$); Ol: Fosterite ($fo_{73}fa_{27}$); Ne: Nepheline ($ne_{77}kls_{13}qtz_{10}$).

PLATE 2 (opposite page)
Photomicrographs of selected pegmatoid and xenolith textures within the Round Lagoon nephelinite. Field of view for each image, 5 mm wide X 3.5 mm high. A. Wehrlite (RL8), with olivine (large grains), Cr-rich augite (long crystals, centre and bottom left) and Cr-bearing spinel (opaque grain, centre top). B. Olivine-nepheline-clinopyroxenite (RL 19) with diopside (large grains) riddled with olivine (small crystals, light and dark altered grains) and nepheline (light coloured crystals). C. Sodalite ijolite (RL3) with nepheline and sodalite (light crystals), diopside (spongy included cores), Ti-rich diopside (rims), aegirine-augite (dark overgrowths, bottom right) and ulvospinel (opaque interstitial crystals, top). D. Ijolite (RL2A), with nepheline and anorthoclase (light crystals), strongly zoned Ti-rich diopside (dark crystals). E. Nepheline syenite (RL6), with nepheline (light aligned crystals),sanidine (light coloured enclosure, centre left), diopside (intergrown darker area) and ulvospinel (large crystals, bottom left). F. Alkali syenite (RL15) with sanidine (light aligned crystals), diopside (small crystals top centre) and aegirine-augite and aegirine (dark intergrowth). G. Spinel meta-lherzolite (RL9) with olivine (large crystal, centre bottom), diopside (crystal centre top) and orthopyroxene (centre right and top left). H. Altered meta-wehrlite (RL6A) with olivine (crystals top right and bottom left), diopside (crystals bottom right), Cr-bearing spinel (black irregular grains) and extensive fine grained recrystallised zones. All images taken in plane polarised light. R.E. Pogson photographer.

TABLE 3
Representative mineral analyses, ijolitic pegmatoids

Analysis wt.%	Sodalite ijolite (RL3)					Ijolite (RL2A)				
Mineral	Ne	Sdl	Cpx[1]	Cpx[2]	Ol	Nep	Afd	Cpx	Ol	Spl
SiO_2	42.10	38.19	54.73	51.60	37.20	42.18	62.73	47.47	37.42	0.65
TiO_2			0.20	3.97			0.44	3.42	0.02	21.26
Al_2O_3	33.19	30.89	0.22	0.35	0.03	34.26	20.71	4.95	0.05	0.60
Cr_2O_3			0.12					0.09	0.05	0.77
FeO	1.04	0.72	5.98	16.67	28.56	0.86	0.38	7.36	21.70	46.38
Fe_2O_3				7.12						27.39
MnO		0.01	0.12	0.09	0.85	0.03	0.01	0.20	0.54	0.61
MgO	0.39		14.89	3.24	31.67	0.17	0.01	12.50	39.15	2.74
CaO	0.06	0.10	24.04	7.19	0.74	1.64	1.29	23.55	0.52	0.79
Na_2O	14.00	21.89	0.14	9.29		16.40	6.62	0.46		
K_2O	8.72	2.39	0.09			4.50	5.87	0.02		
Cl		7.37								
O≡Cl		−1.66								
Total	99.50	99.89	100.53	99.49	99.05	100.04	98.06	100.29	99.45	101.19
Cations (No. O)	32	26 (+Cl)	6	6	4	32	32	6	4	32
Si^{4+}	8.239	6.179	2.008	1.982	1.012	8.109	11.496	1.774	0.981	0.188
Ti^{4+}			0.006	0.115			0.061	0.096	0.000	4.634
Al^{3+}	7.655	5.890	0.010	0.016	0.001	7.763	4.473	0.218	0.002	0.205
Cr^{3+}								0.003	0.001	0.177
Fe^{2+}	0.17	0.097	0.184	0.229	0.650	0.138	0.058	0.156	0.476	11.243
Fe^{3+}				0.482				0.074		5.974
Mn^{2+}		0.001	0.004	0.003	0.020	0.005	0.002	0.006	0.012	0.150
Mg^{2+}	0.114		0.814	0.186	1.284	0.049	0.003	0.696	1.530	1.184
Ca^{2+}	0.013	0.017	0.945	0.296	0.022	0.338	0.253	0.943	0.015	0.245
Na^{1+}	5.312	6.867	0.010	0.692		6.113	2.352	0.035		
K^{1+}	2.177	0.493	0.004			1.104	1.372	0.001		
Cl		2.021								
Sum	23.680	21.565	3.989	4.001	2.989	23.619	20.070	4.002	3.017	24.000
Cation ratio (%)										
Mg			42.0	11.7	64.9			37.2	76.1	11.3
Fe			9.3	44.8	35.0			12.3	23.9	73.1
Ti										15.6
Ca	0.1	0.2	48.7	43.5	0.1	4.5	6.3	50.5	0.0	
Na	70.8	93.2				80.9	59.2			
K	29.0	6.6				14.6	34.5			

RL3 Ne: Nepheline ($ne_{67}kls_{30}qtz_3$); Sld: Sodalite ($sld_{93}k\text{-}sld_7$); Cpx[1]: Diopside ($wo_{49}en_{42}fs_9$); Cpx[2]: Aegrine-augite ($acm_{54}wo_{20}en_{15}fs_9jd_2$); Ol: Forsrerite ($fo_{65}fa_{35}$);
RL2A Ne: Nepheline ($ne_{83}kls_{15}qtz_{22}$); Afd: Anorthoclase ($ab_{59}or_{35}an_6$); Cpx: Diopside ($wo_{51}en_{37}fs_{12}$); Ol: Forsterite ($fo_{76}fa_{24}$); Spl: Ulvospinel ($usp_{60}mag_{19}mf_{18}hc_1chr_1$)

Al_2O_3 1–7 wt.%). Ulvospinel ($usp_{42-61}mf_{17-33}mag_{8-20}hc_{1-14}chr_{1-4}$) forms sparse, large anhedral grains and is also present as inclusions in olivine (fo_{76-78}). Apatite is common as inclusions in the diopside.

Syenitic pegmatoids

These occur as nepheline-bearing and nepheline-free syenitic assemblages. The nepheline-bearing assemblages (RL2A, 7A, 11; table 4, pl. 2D) are dominated by coarse-grained, zoned subhedral to euhedral prismatic, pale brown to green rimmed, Ti-Al-bearing diopside ($wo_{48-51}en_{38-42}fs_{10-12}$;$TiO_2$ 1.9–3.0 wt.%, Al_2O_3 3.0–6.5 wt.%). The central parts of these are crowded with inclusions, some being forsteritic olivine, and some outer rims pass into green sodic pyroxenes. The pyroxenes are embedded in coarse-grained, zoned sodic sanidine ($or_{52-53}ab_{4-47}an_1$), subhedral nepheline ($ne_{81-83}kls_{14-5}qtz_{3-5}$) and ulvospinel ($usp_{47-55}mag_{27-34}mf_{19-34}hc_{0-1}chr_{0-1}$) grains. Subordinate mesostasis and brown glass contain apatite and traces of biotite.

Syenites lacking nepheline (RL15; table 4, pl. 2F) are relatively rare among the pegmatoids. Some contain orientated, partly radial, intergrowths of sanidine laths ($or_{48-52}ab_{47-51}an_{0-1}$) and elongate diopside blades ($wo_{48-49}en_{41-42}fs_{9-10}$; TiO_2 up to 1.2 wt.%). The diopside develops outer rims and tips of more sodic green to dark green pyroxenes with compositions of aegirine-augite ($acm_{23-38}jd_{0-2}cf_{0-2}wo_{29-35}en_{22-29}fs_{9-11}$) and aegirine ($acm_{78-83}jd_{2-3}wo_{11}en_{6-10}fs_0$). Accessory green-brown amphibole grains range from titanian richterite and titanian ferro-richterite to potassic-titanian-richterite and titanian-magnesiokatophorite.

TABLE 4
Representative mineral analyses, ne-syenitoid and syenitoids

Analysis wt.%	Nepheline syenite (RL6)					Alkali syenite (RL15)				
Mineral	Afd	Ne	Cpx	Spl	Ol	Afd	Cpx[1]	Cpx[2]	Cpx[3]	Amp
SiO_2	66.29	44.06	51.31	0.66	38.62	65.80	53.98	51.34	50.65	50.84
TiO_2	0.24		2.15	15.95		0.32	0.26	1.38	3.31	4.76
Al_2O_3	18.75	33.51	3.04		0.22	18.12	0.44	0.33	0.36	1.21
Cr_2O_3			0.19							
FeO	0.72	0.88	6.13	40.30	22.01	1.56	3.92	5.49	0.00	14.33
Fe_2O_3				38.44			2.37	12.88	26.35	
MnO				1.03	0.46		0.20	0.31	0.15	0.16
MgO			13.94	3.38	38.46	0.12	15.07	7.82	3.35	13.15
CaO	0.18	0.54	23.17	0.15	0.82	0.04	24.38	14.25	5.04	4.97
Na_2O	5.31	16.93	0.56			5.47	0.54	5.26	11.39	6.92
K_2O	8.99	4.36				8.55	0.02	0.08	0.03	1.38
Total	100.48	100.29	100.49	99.91	100.59	99.98	100.94	99.14	100.63	97.72
Cations (No. O)	32	32	6	32	4	32	6	6	6	23
Si^{4+}	11.932	8.396	1.892	0.195	0.999	11.937	1.981	1.964	1.911	7.514
Ti^{4+}	0.032	7.528	0.060	3. 538		0.044	0.007	0.040	0.094	0.529
Al^{3+}	3.980	0.140	0.132		0.007	3.874	0.019	0.015	0.016	0.211
Cr^{3+}			0.006							
Fe^{2+}	0.018		0.189	9.942	0.476	0.237	0.120	0.176	0.000	1.771
Fe^{3+}				8.534			0.065	0.371	0.748	0.000
Mn^{2+}				0.257	0.010		0.006	0.010	0.005	0.020
Mg^{2+}			0.766	1.486	1.483	0.032	0.820	0.446	0.188	20897
Ca^{2+}	0.036	0.112	0.915	0.047	0.023	0.008	0.954	0.584	0.204	0.787
Na^{1+}	0.463	6.256	0.040			1.924	0.038	0.390	0.833	1.983
K^{1+}	1.852	1.060				1.979	0.001	0.004	0.001	0.260
Sum	20.004	23.496	4.000	27.455	2.997	20.035	4.001	4.000	4.000	15.972
Cation ratio (%)				23.981						
Mg			41.0	6.3	74.9		41.6	28.4	11.4	43.7
Fe			10.1	78.5	24.0		9.6	34.6	41.9	26.4
Ti				15.1						
Ca	0.9	1.5	48.9		1.1	0.3	48.7	37.0		
Na	46.9	84.2				49.2			46.7	29.9
K	52.2	14.3				50.5				

RL6 Afd: Sanidine ($or_{52}ab_{47}an_1$); Ne: Nepheline ($ne_{81}kls_{15}qtz_5$); Cpx: Diopside ($wo_{49}en_{41}fs_{10}$); Spl: Ulvospinel ($usp_{47}mag_{34}mf_{19}$); Ol: Forsterite ($fo_{75}fa_5$).
RL15 Afd: Sanidine ($or_{51}ab_{49}an_0$); Cpx[1]: Diopside ($wo_{49}en_{42}fs_{10}$); Cpx[2]: Aegirine-augite ($acm_{37}wo_{29}en_{22}fs_9jd_2$); Cpx[3]: Aegirine ($acm_{78}wo_{11}en_{10}jd_2fs_0$); Amp: Potassian-titanian-richterite.

Mantle meta-assemblages

These coarse-grained metamorphic assemblages are mostly spinel meta-lherzolite, but include spinel meta-wehrlite and spinel meta-websterite. The spinel meta-lherzolites (RL9, RL18, table 5, pl. 2G) consist of anhedral aggregates of olivine (fo_{88-89}), Al-Cr-bearing diopside ($wo_{50-52}en_{44-46}fs_{4-5}$; Al_2O_3 5.0–5.2 wt.%, Cr_2O_3 0.8–1.0 wt.%) and Al-bearing enstatite ($en_{88-89}fs_{10-11}wo_1$), interspersed with accessory Cr-bearing spinel ($spl_{70}chr_{14}hc_7$). The enstatite includes blebs and lamellae of Al-bearing diopside ($wo_{48-50}en_{45-47}fs_5$; Al_2O_3 5 wt.%), which gave estimated metamorphic re-equilibration temperatures of 890–950°C (Wells 1977, two-pyroxene Fe^{2+} thermometry).

Spinel meta-wehrlites (RL6A; table 5; pl. 2H) contain anhedral olivine (fo_{88-89}) and Cr-Al-bearing diopside ($wo_{49-50}en_{46-47}fs_4$; Al_2O_3 1.3–2.3 wt.%, Cr_2O_3 1.0–1.1 wt.%) and some interstitial Cr-bearing spinel ($spl_{73}chr_{10}hc_9mag_6$). The diopsides are spongy and partly replaced by melting reactants.

Many of the metamorphic assemblages show considerable recrystallisation and alteration related to reactions with fluid infiltrations from the host nephelinite. Recrystallisation is accompanied by replacement of the coarser phases by small olivine, clinopyroxene and ulvospinel grains, formation of sporadic large anhedral green spinel grains and development of a glassy melt. Initial reaction takes place along grain boundaries, but become more complex as clinopyroxenes and spinels develop sieve texture and orthopyroxene reacts to form replacement rims and glassy melt textures. Similar reactants were described in mantle suites in Boat Harbour, NW Tasmania, olivine nephelinite (Sutherland *et al.* 1996) and the compositions of such products have been reproduced experimentally at low pressure (Shaw & Dingwell 2008).

TABLE 5
Representative mineral analyses, meta-peridotites

Analysis wt.%	Spinel lherzolite (RL9)							Meta-wehrlite (RL6A)		
Mineral	Ol	Cpx	Opx^1	Cpx^1	Opx^2	Cpx^2	Spl	Ol	Cpx	Spl
SiO_2	41.19	52.20	55.23	52.06	54.93	52.06		40.70	54.31	0.37
TiO_2	0.10	0.54	0.13	0.60	0.14	0.63	0.18		0.21	0.16
Al_2O_3		5.03	3.67	4.98	3.76	5.14	56.29		1.28	53.49
Cr_2O_3		1.03	0.34	0.72	0.37	0.83	13.38		1.00	9.97
FeO	11.05	2.78	6.70	2.97	6.72	2.96	9.95	10.72	2.66	12.49
Fe_2O_3							0.23			5.40
MnO	0.19		0.14	0.08	0.25	0.02	0.03	0.22	0.07	0.29
MgO	47.31	14.67	31.77	15.46	31.51	15.16	20.44	48.38	16.34	18.74
CaO		22.59	0.43	22.34	0.39	22.53			24.55	
Na_2O		1.02		0.48		0.76			0.15	0.01
K_2O						0.04			0.04	
Total	99.84	99.86	98.41	99.69	98.07	100.13	100.50	100.02	100.62	100.92
Cations (No. O)	4	6	6	6	6	6	32	4	6	32
Si^{4+}	1.014	1.902	1.937	1.897	1.943	1.892		1.001	1.974	0.078
Ti^{4+}	0.002	0.015	0.003	0.016	0.004	0.017	0.028		0.006	0.025
Al^{3+}		0.216	0.152	0.214	0.156	0.220	13.721		0.055	13.215
Cr^{3+}		0.030	0.009	0.021	0.010	0.024	2.188		0.029	1.652
Fe^{2+}	0.228	0.085	0.197	0.091	0.198	0.090	1.721	0.220	0.081	2.190
Fe^{3+}							0.035			0.930
Mn^{2+}	0.004		0.004		0.008	0.001	0.005	0.005	0.002	0.052
Mg^{2+}	1.737	0.797	1.661	0.840	1.663	0.821	6.302	1.773	0.883	5.856
Ca^{2+}		0.882	0.016	0.872	0.015	0.877			0.954	
Na^{1+}		0.072		0.034		0.054			0.011	
K^{1+}						0.002			0.002	0.003
Sum	2.985	3.999	3.979	3.99	3.997	3.998	24.000	2.999	3.997	24.000
Cation ratio (%)										
Mg	88.3	45.5	88.5	46.7	88.7	45.8	61.5	88.9	46.1	55.1
Fe	11.7	4.5	10.6	5.0	10.5	5.0	17.1	11.1	4.2	29.3
Ca	0.0	50.0	1.1	48.3	0.8	49.2		0.0	49.7	
Cr							21.3			15.6

RL9. Ol: Forsterite ($fo_{88}fa_{12}$); Cpx: Diopside ($wo_{50}en_{46}fs_5$); Opx^1: Enstatite ($en_{89}fs_{11}wo_1$); Cpx^1: Diosipde ($wo_{48}en_{47}fs_5$); Opx^2: Estatite ($en_{89}fs_{11}wo_1$); Cpx^2: Diopside ($wo_{49}en_{46}fs_5$); Spl: Cr-rich spinel ($sp_{79}cm_{14}hc_7$). Opx^1-Cpx^1 Wells two-pyroxene (Fe^{2+}) T 947°C; Opx^2-Cpx^2 Wells two-pyroxene (Fe^{2+}) T 890°C

RL6A Ol: Forsterite ($fo_{89}fa_{11}$); Cpx: Diopside ($wo_{50}en_{46}fs_4$); Spl: spinel ($spl_{73}chr_{10}hc_9mag_6usp_6$).

DISCUSSION

The Round Lagoon nephelinite and contained coarse assemblages suggest its magmatic evolution took place under at least two different pressure-temperature regimes. The cumulate wehrlite and ol-clinopyroxenite bodies in the mantle meta-lherzolite xenolith (fig. 1) suggests a higher pressure, shallow mantle stage. Other cognate ultramafic to mafic assemblages, however, have mineral compositions similar to those in the host nephelinite that relate to later, lower pressure crystallisation.

Host nephelinite

This is a K-rich olivine nephelinite with a low $^{87}Sr/^{86}Sr$ (0.7302 ± 3) and is isotopically typical of many Tasmanian undersaturated alkaline lavas (McDonough *et al.* 1985, Sutherland 1989). In the spectrum of strongly undersaturated alkaline lavas in Tasmania, it has high SiO_2 content suggesting transition into basanite (fig. 2). The analysis has a high, near-primary Mg# (0.66), and relatively high Ni (341 ppm) and Cr (550 ppm). These apparently near-primary characteristics, however, are probably misleading due to many inextricable small xenocrysts of olivine and pyroxene, thus the rock does not represent a liquid composition. The magma was probably mildly fractionated, based on its olivine phenocryst compositions (up to fo_{78} which would be in equilibrium with a liquid of Mg # 0.51–0.52) and its relatively elevated incompatible elements; for example it has a Zr content (460 ppm) compared to Zr contents (<370 ppm) in other primary olivine nephelinites in Tasmania (Sutherland 1989, Sutherland *et al.* 1996, Sutherland *et al.* 2004, J. Everard, unpubl. data base). Available trace element data normalised to primitive mantle contents (fig. 3) compare closely with patterns for a fractionated olivine nephelinite (Mg# 0.59) and mantle-derived basanite (UT704489) from the Midlands area, and are higher in most of these elements than nephelinites from Boat Harbour. Based on the occurrence of the cumulate wehrlite and olivine clinopyroxenite found within the mantle xenolith suite, such fractionation was probably initiated at

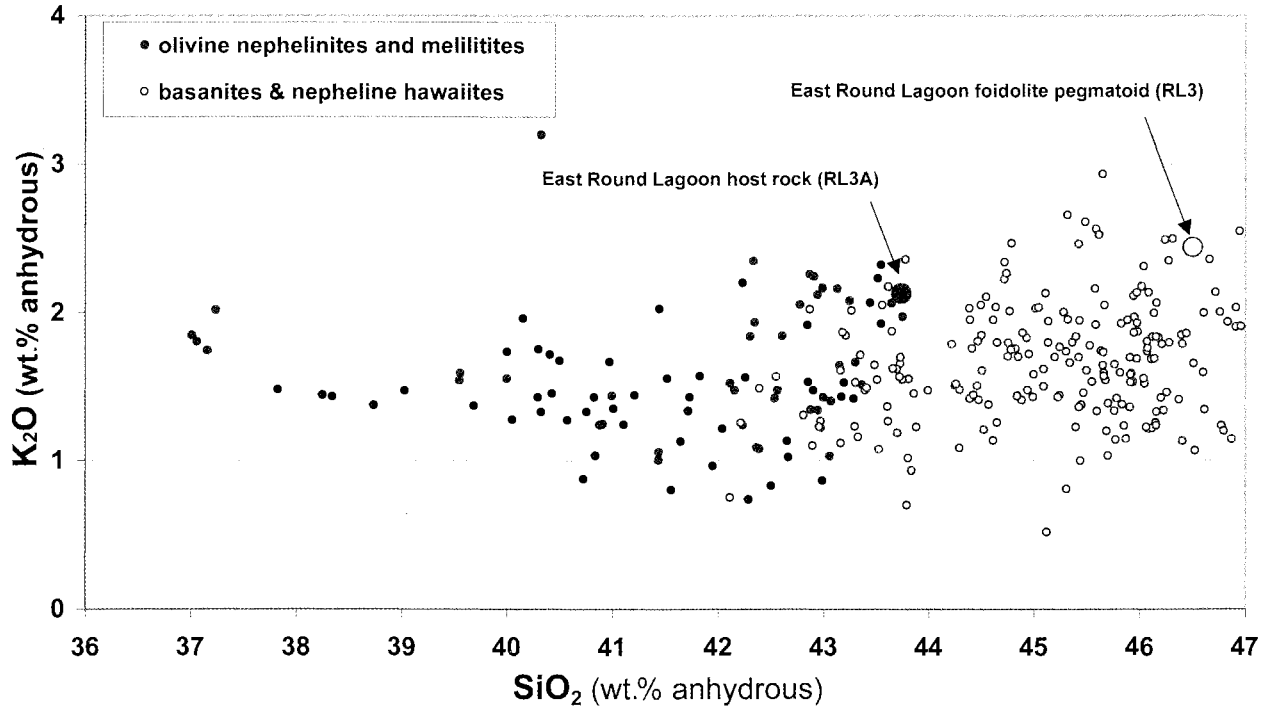

FIG. 2 — Alkali (K_2O) – SiO_2 (anhydrous) plots for Tasmanian melilitites and nephelinites, in relationship to the Round Lagoon nephelinite and sodalite ijolite (larger circles).

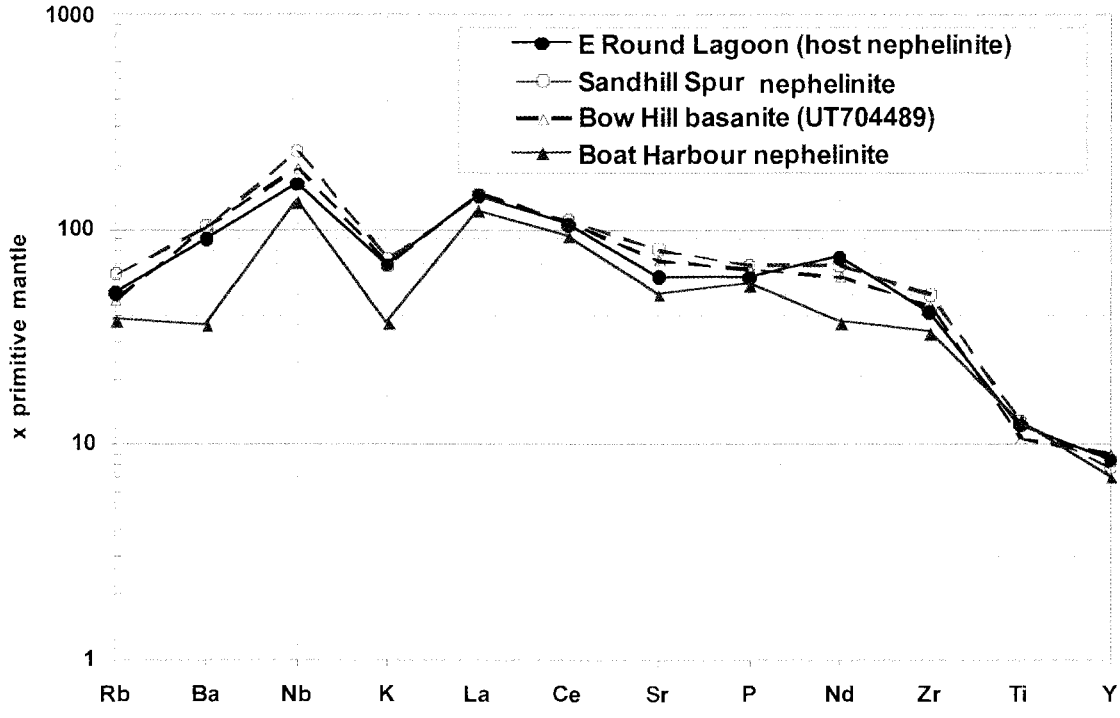

FIG. 3 — Incompatible multi-element plots for Round Lagoon nephelinite in comparison to other Tasmanian nephelinites and transitional basanites. Normalising factors are after Sun & McDonough (1989). Other data sources: Sandhill Spur (Sutherland et al. *2004), Bow Hill (Adam 1990) and Boat Harbour (Sutherland* et al. *1996).*

mantle depths under the site, although detailed rare earth element and isotopic analyses of both host and cumulate xenoliths are needed to confirm this. The mantle peridotites indicate a fast ascent of the nephelinite host, probably in the range of 10^{-2} to 5 m/s (Spera 1984). A primary composition of the original nephelinite magma could be provisionally estimated by adding in Mg-rich olivine, clinopyroxene ±spinel compositions found in wehrlite cumulates within the host nephelinite (table 2).

As proportions of such liquidus phases are only broadly constrained, two potential extracts were calculated; one had abundant olivine (65%), moderate clinopyroxene (30%) and accessory spinel (5%); the other had clinopyroxene (65%) dominant over olivine (30%), with accessory spinel (5%). The mineral compositions added from table 2 give potential magma compositions at 10% and 20% liquidus crystallisation. The olivine-dominant scheme gave Mg # 0.73 and 0.76 respectively, with high normative ol (24–28%), di (27–28%) and ne (13–15%) and or (10%). The clinopyroxene-dominant scheme gave Mg# 0.72 and 0.74 respectively, lesser normative ol (21–28%) to di (30–35%), but similar ne (14–15%) and or (10–12%) ranges. The latter parents resemble primitive mantle-derived olivine nephelinite (Mg # 0.73–0.75) in young Tasman Sea volcanism (Briggs *et al.* 1997).

The above calculated parent compositions would be partly modified under mantle conditions, in which more Al-Na-rich clinopyroxene typifies high-pressure liquidus phases. In ne-rich rocks and experimental runs on Tasmanian and other nephelinites such clinopyroxenes contain up to 10 wt.% Al_2O_3, 4 wt.% TiO_2 and 2 wt.% Na_2O (Bultitude & Green 1971, Fodor *et al.* 1982, Adam 1990, Sutherland *et al.* 1996, 2004, 2005, Woodland & Jugo 2007). Thus, a Round Lagoon mantle parent would have higher Al, Ti and Na than estimated from the low-pressure wherlitic extracts, but would be compatible with a high-pressure fractionation series in which sodic nephelinite magmas evolve to more K-rich members (Sutherland 1974). The Round Hill nephelinite, when adjusted for hydrous content, is near a Bow Hill, Tasmanian basanite in composition, which experimentally crystallised clinopyroxene at P>2.6 GPa and clinopyroxene and olivine at lower pressures in runs at 1270°C and 4.5 wt.% H_2O (UT-70489, Adam 1990). Based on such experimental work (Adam 1990, Green & Falloon 1998), the Round Lagoon magma probably segregated at 3 GPa (90 km depth) under low degrees of partial melting of garnet lherzolite that contained <7 wt.% volatiles (H_2O + CO_2). The nephelinite has high Ba, and to a lesser degree high Zr, Nb, and K. The Ba/Zr (1.4) and Ba/Nb (5.4) ratios are relatively high compared to some other Tasmanian nephelinites (Ba/Zr<1, Ba/Nb>3); which suggests either amphibole was low in the mantle source (Chazot *et al.* 1996), or that its contribution to the magma became diluted through the suspected mantle fractionation.

The lack of garnet or its replacements in Round Lagoon inclusions suggests the magma stalled and fractionated at mantle levels shallower than the spinel-garnet lherzolite transition, i.e., <1.7–1.8 GPa and 1100–1200°C for Tasmanian Miocene geotherms (Sutherland *et al.* 2005). The two-pyroxene temperatures for Round Lagoon spinel meta-lherzolite reach 950°C (table 5). Based on the Tasmanian geotherm, this suggests magma began to fractionate at around 1.0–1.1 GPa (30–35 km), at mantle depths shallower than the spinel-garnet pyroxenite transition. This agrees with a Moho depth at 30 km below the area. At these pressures, using the calculated CaO/(CaO+MgO) ratio of the nephelinite parental magma, the liquidus phases crystallising during this mantle fractionation would favour significant olivine along with clinopyroxene (Smith *et al.* 2008).

Low-pressure crystallisation

Clinopyroxenes in the Round Lagoon cumulate and pegmatoid assemblages mostly show relatively high Al^{IV}/Al^{VI} ratios (1.5–13.5). Such ratios typically indicate low-pressure igneous crystallisation, rather than mantle and lower crust pressures (Wass 1979, Mason 1985, Simonetti *et al.* 1996). The mantle xenolith clinopyroxenes give ratios of 1 or less, but some from wehrlitic cumulates have transitional values. Amphiboles in the pegmatoids also show high Al^{IV} and Ti, features that were found in lower pressure experimental runs of strongly undersaturated magmas (Adam *et al.* 2007).

Ultramafic crystallisation

Initial temperatures for crystallising liquidus minerals from such nephelinite magmas are about 1300°C for olivine, 1150°C for clinopyroxene and 1065°C for nepheline (Wilkinson 1977). These intervals cover the wehrlite (RL8) and ol-ne-bearing clinopyroxenite (RL19) assemblages. Olivine is highly magnesian (fo_{90-91}) in the wehrlites but less so in the clinopyroxenites (fo_{73}); the latter contains minor Ca_2SiO_4 and Mn_2SiO_4 end member components. Clinopyroxenes are Na-Cr-enriched augites in the wehrlites, but these elements are lower, and Ca and Fe higher in the diopside of the clinopyroxenites. Early nepheline in the clinopyroxenites is sodic (ne_{76-77}), and compositions suggest crystallisation around 980°C, based on experimental isotherms (Hamilton 1961). Estimates for crystallisation temperatures from nephelines, however, may be minimum values due to potential exchanges of alkalis and aqueous vapour that reset them to lower kls and qtz and so apparently lower temperatures (Edgar 1984).

Residual glass in the clinopyroxenites has an alkaline trachytic composition (table 6). Normatively this corresponds to minor Q (3%), Ab-rich plagioclase (43%) and Or (47%), together with accessory Hy, C, Mt and Il. Removal of MgO (1.9 wt.%) and FeO (1.2 wt.%) in the glass to crystallise spinel, leaves a remainder close to alkali feldspar in composition, with a stoichiometric formula approximating anorthoclase ($ab_{77}or_{21}an_2$). A potential spinel-bearing, anorthoclase-rich crystallisation from this glass is compatible with such phases observed in the more evolved pegmatoid (RL2A).

Main mafic crystallisation

Depletion of Mg, Ca and Fe and accumulation of alkalis and volatiles in the magma then produced sodic feldspathoidal-rich assemblages, such as sodalite-ijolite (RL3). Nepheline (Ne_{67-68}) in the sodalite-ijolites (RL3) is richer in K than in the nepheline-dominant ijolite (RL2A) and syenite (RL6) (fig. 4), as crystallising sodalite would compete for Na. Its composition suggests formation near 700°C based on experimental isotherms (Hamilton 1961). With up to 20% sodalite crystallisation, Cl was a significant volatile in the system. Crystallising pyroxene was accordingly Na-poor diopside, but incorporated Fe, Ti and Na to form late aegirine-augite (acm_{53-57}).

As feldspathoid crystallisation diminished, alkali feldspar ($ab_{59-61}or_{33-35}an_{6-7}$) became more important (fig. 4) in ijolitic assemblages (RL2A). Nepheline became more

TABLE 6
Major and trace element analyses, nephelinite host, foidolite and cumulate glass

Analysis	Major elements, CIPW norms and Indices			Trace elements (ppm)		
Oxides (wt.%)	Nephelinite[1]	Foidolite[1]	Glass[2]		Nephelinite[1]	Foidolite[1]
SiO_2	42.28	45.95	64.59	Cr	550	86
TiO_2	2.65	2.50	0.20	Ni	341	125
Al_2O_3	10.81	13.03	17.36	V	112	290
Fe_2O_3	3.94	4.92	0.21			
FeO	8.61	4.57	1.03	Ba	625	1100
MnO	0.20	0.15		Y	38	38
MgO	11.35	7.95	1.90	Sr	1269	1850
CaO	9.83	12.67	0.17	Zr	460	520
Na_2O	4.03	3.89	4.88	U	<2	<5
K_2O	2.06	2.41	7.81	Rb	32	68
P_2O_5	1.30	1.26		Th	9	<4
H_2O+	2.49	0.14		Pb	27	8
CO_2	0.28	0.37		Ga	24	19
Total	99.83	99.81	98.15	Nb	115	210
Na_2O/K_2O	1.96	4.10	0.62			
CIPW Norm (anhydrous, based on Fe_2O_3/FeO = 0.2)				La	98	NA
				Ce	187	NA
Q			2.53	Nd	100	NA
Or	12.56	14.38	47.02			
Ab	3.36	5.18	42.07	Zn	175	93
An	5.49	11.08	0.86	Cu	57	70
Ne	17.24	15.20	Hy 6.24			
Di	29.14	33.59		Trace element ratios		
Ol	20.77	8.53		Cr/Ni	1.613	0.689
Mt	3.08	2.23	0.31	Rb/Sr	0.025	0.037
Il	5.17	4.80	0.39	Zr/Nb	4.000	2.477
Ap	3.16	3.16		Ba/Nb	5.435	5.238
Other			C 0.58	Rb/Nb	0.278	0.324
				Th/U	>4.50	>0.80
				La/Y	2.5	
				Ce/Y	4.9	
Mg/ Mg+Fe^{2+}	0.663	0.650	0.766			
ΣOr, Ab, Ne, Q	33.16	34.76	91.62			
An mol. %	60.63	66.83	2.00			

Major and trace element analyses (RL3A, RL3) after Forsyth (1989)[1] and (RL 19)[2] this paper.

sodic (ne_{82-83}), with compositions suggesting T <500°C, based on experimental isotherms. Clinopyroxene remained diopsidic, but became more Ti- and Fe-rich. Mg-bearing ulvospinel (usp_{42-60}) formed the distinct Fe-Ti oxide. Such assemblages crystallising from hydrous nephelinitic magma would begin at around 880–890°C at 0.1 GPa, based on the diopside-albite-nepheline phase relationships (Patic *et al.* 2000) assuming sodic anorthoclase and albite are relatively close in composition. This is higher than the T indicated by the nepheline compositions, but the latter may be low due to hydrous vapour exchanges.

Feldspathic crystallisation

Alkali feldspar formed a principal K-rich phase (sanidine, or_{52-53}) in these assemblages (RL6), as Si, Ti, Fe and alkalis, particularly K, became concentrated with fractionation. Although subordinate, olivine remained magnesian (fo_{75}) while nepheline remained sodic (ne_{81-83}) with a composition similar to the low T (<500°C) nepheline in the host nephelinite. Clinopyroxene is Ti-enriched diopside and ulvospinel (usp_{47}) is the accessory oxide.

In the most evolved assemblages, K-rich alkali feldspar (or_{49-52}) appears without nepheline in alkali syenites (RL15). Clinopyroxenes enriched in Ti, Fe and Na on their rims, pass from strongly zoned diopside (fig. 5), through aegirine-augite (acm_{23-37}) into aegirine (acm_{78-83}). Amphiboles in the hydrous residues are K- and Ti- rich richterites. They are deficient in their cation sites, regardless of element and Fe valency assignments. Other elements not analysed in the EMP array may be present, as detected in certain amphibole associations elsewhere (Eggins *et al.* 1998, Preston *et al.* 2000), but such assignments remain problematic.

The feldspathic assemblages are commonly subspherical with the main phases radiating inwards from the margins, suggesting cavity infilling during final consolidation of the nephelinite. This contrasts with the irregular and vein-like mafic assemblages. These feldspathic residues resemble invariant point equilibrium assemblage compositions found for nephelinite-like compositions in the experimental diopside-albite-nepheline system at $P(H_2O)$ = P(Total) = 0.2 GPa (Patic *et al.* 2000).

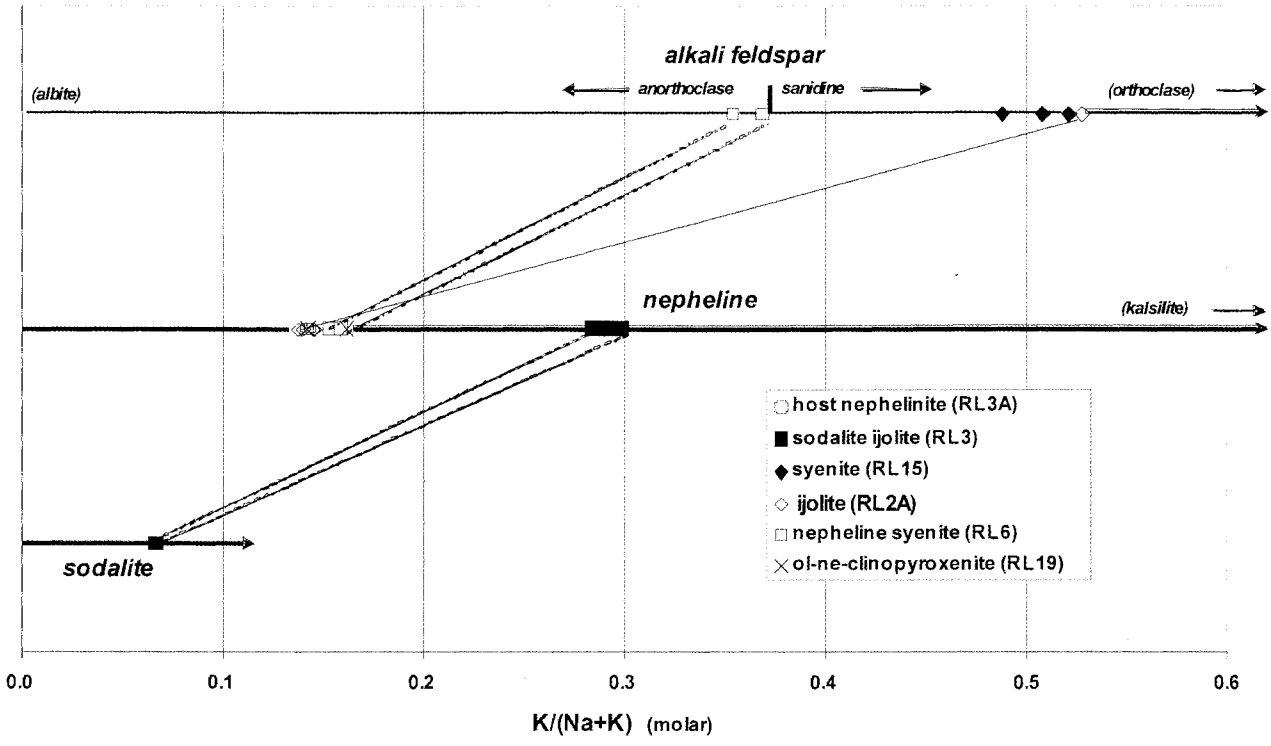

FIG. 4 — Plots of feldspathoid and feldspar compositions, from Round Lagoon nephelinite and pegmatoids: K/(Na + K) molar values for alkali feldspar, nepheline and sodalite, with symbols shown in legend for different samples. The various connecting lines link co-existing phases in the same sample.

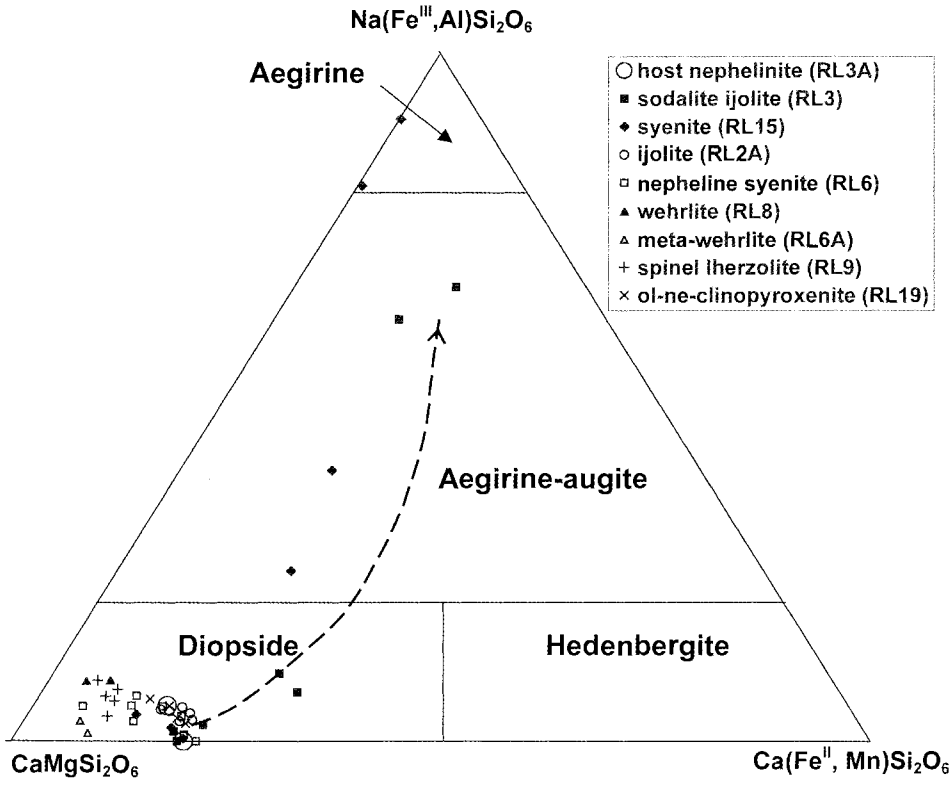

FIG. 5 — Compositional plots, Round Lagoon analysed pyroxenes, on a triangular end member Diopside – Hedenbergite – Aegirine diagram, with symbols after listed samples. The trend line of increasing Na is from analyses for Inverell, NSW, nephelinite and pegmatoids shown by Wilkinson (1977).

Fractionation sequence

The mineral paragenesis in the Round Lagoon fractionates suggests progressive, but discontinuous, crystallisation of assemblages within a cooling solidifying nephelinite magma, as follows: Wehrlites → Olivine-clinopyroxenites → Sodalite-ijolites → Ijolites → Nepheline syenites → Alkali syenites. Within this series, Mg depletion took place in olivines (fo_{91} → fo_{67}) and clinopyroxenes (en_{55} → en_6), which became more Na and Fe-rich (acm_0 → acm_{83}). Accessory oxides were spinel (spl_{83} → spl_1; chr_{14} → chr_1) in ultramafic associations and magnetite-ulvospinel (mag_1 → mag_{34}; usp_2 → usp_{61}) in mafic and feldspathic associations.

Bulk analyses of the host and cognate assemblages are limited in this study, but a sodalite-ijolite analysis (table 6) defines some trends in major element composition with low-pressure fractionation (fig. 2). The depletions in Cr and Ni and enrichments in incompatible elements such as Ba, Sr, Rb, Zr and Nb reflect olivine, pyroxene and spinel crystallisation. The host and sodalite-ijolite bulk compositions do not show extensive separation related to prolonged olivine-clinopyroxene-nepheline crystallisation within the phase equilibrium nepheline-diopside-silica system (Wilkinson 1977). This may suggest rapid, non-equilibrium conditions prevailed during sodalite-ijolite crystallisation, probably initiated by a Cl-rich flux, perhaps accompanied by some magma mixing.

Comparisons with other nephelinite pegmatoids

Examples of pegmatoids in nephelinites in Tasmania, eastern Australia and basalt fields elsewhere are sparse (London 2008). Pegmatoids are also recorded in melilite-bearing or basanitic hosts as in the Shannon Tier melilitite and Table Cape teschenite (Sutherland *et al.* 2004). Transitional basanite nephelinites also contain coarse-grained differentiations (Wittke & Holm 1996). These pegmatoids, however, involve further Ca-rich phases such as melilite or plagioclase in their fractionation and only simpler nephelinite fractionates are considered here.

Australia

Pegmatoids in Tasmanian nephelinites are recorded at Boat Harbour, East Arm (Tamar River) and West Scottsdale, but detailed mineral analyses are only available for the Boat Harbour pegmatoid. That pegmatoid is transitional in mode between Round Lagoon sodalite-ijolite (RL3) and nepheline-syenite (RL6). Sodalite is less potassic ($k\text{-}sdl_1$ *cf* $k\text{-}sdl_7$), nepheline is intermediate in K-content (kls_{19} *cf* $kls_{15\text{-}30}$) and alkali feldspar is more potassic (or_{21} *cf* $or_{53\text{-}59}$), while clinopyroxene has higher Mg (en_{47} *cf* $en_{41\text{-}42}$) and olivine intermediate Mg (fo_{72} *cf* $fo_{64\text{-}75}$), compared to Round Lagoon phases. Nepheline compositions suggest similar crystallisation temperatures to those in the sodalite-ijolite pegmatoid at Round Lagoon (~700°C).

Melanocratic and leucocratic pegmatoids at Inverell (Wilkinson 1977) respectively resemble ijolite (RL2A) and nepheline-syenite (RL6) at Round Lagoon. Inverell melanocratic variants, however, have less sodic nepheline (ne_{79} *cf* ne_{83}) and more potassic alkali feldspar ($or_{57\text{-}64}$ *cf* $or_{37\text{-}52}$), while clinopyroxenes have lower Ti and Al and olivine has lower Mg (fo_{60} *cf* fo_{67}). Nepheline compositions suggest formation at ~500°C, compared to <500°C at Round Lagoon.

Inverell host nephelinite is more evolved than Round Lagoon nephelinite (Mg # 0.63 *cf* 0.66), but has a similar Na_2O/K_2O ratio (1.95 *cf* 1.96, table 6). The higher Ca and Al contents in the Inverell nephelinite may reflect its more olivine-dominated fractionation, but other magmatic differences may also apply.

An alkaline pegmatoidal clot found in a Victorian nephelinite differs from the Tasmanian examples in lacking nepheline and containing quartz, giving it a problematic relationship to its host (Ferguson 1977).

Argentina

A well studied nephelinite-pegmatoid exposure at La Madera, Córdoba (Galliski *et al.* 2004), is derived from a more primitive parental magma than for the Australian examples (Mg#0.70 *cf* 0.63–0.66). The presence of both melanocratic and leucocratic pegmatoids parallels the Inverell situation more closely than the more diverse assemblages at Round Lagoon. La Madera melanocratic assemblages are closest to Round Lagoon ijolites (RL2A), but lack sodalite, alkali feldspar and olivine. La Madera nephelines are more potassic ($Ks_{30\text{-}34}$ *cf* $Ks_{15\text{-}30}$), while the Ti, Al, Na-bearing diopsides and Ti-rich magnetites overlap the Round Lagoon mineral compositions. The pyroxenes show Na and Fe^{3+} enrichment trends, but do not extend to aegirine as in the extreme Round Lagoon fractionates. Amphiboles have less Si and more Ti and K than Round Lagoon amphiboles, and are mostly katophorites rather than richterites.

Nepheline compositions in La Madera pegmatoids give more restricted T crystallisation ranges than Round Lagoon pegmatoids (750–800°C *cf* <500–980°C). Other mineral phases, not recorded in Round Lagoon assemblages, include perovskite, analcime and phillipsite-Na. The leucocratic pegmatoids at La Madera are hydrous and carbonated assemblages that indicated liquid immiscibility, a process less evident in Round Lagoon fractionation. Although injected in surface extrusions, La Madera pegmatoids provide insight into subsurface fractionation at Round Lagoon.

Round Lagoon low-P magmatic evolution

The various pegmatoids in the nephelinite demonstrate a stepped fractionation process. Separation of Mg-rich olivine, Mg-Ca-rich clinopyroxene and Mg-rich spinel during initial cooling from 1140°C depleted the magma in considerable Mg and some Ca. The greater activity of MgO over that of other oxides expands the diopside field (Deer *et al.* 1997a, Gallisky *et al.* 2004), so that wehrlitic cumulates gave way to olivine clinopyroxenite cumulates. A change, from Cr- and Mg-rich clinopyroxene to more calcic clinopyroxene, introduced two separate pyroxene components into the pegmatoid sequence. Differences in clinopyroxene phenocryst compositions related to changes in magma chamber compositions are known from phenocrysts generated below nephelinite volcanoes (e.g., at Napak volcano; Simonetti *et al.* 1996), but the precise causes that produced the two distinct Round Lagoon types (Cr- and Na-bearing augite and Ti- and Al-bearing diopside) await more detailed study. As alkalis and Fe increased in the evolving magma and temperatures dropped below 1000°C, nepheline became an important crystallising phase and the pyroxene composition moved towards aegerine-augite, rather than less stable hedenbergite (Galliski *et al.* 2004). With Al entering into nepheline, distinct changes in oxide crystallisation favoured ulvospinels over spinels.

As Si contents increased, alkali feldspar joined the other crystallising phases to form ijolites and nepheline syenites. These solidified below 850°C, as typifies lower temperature derivatives observed in the diopside-albite-nepheline experimental system (Patic *et al.* 2000). Such assemblages crystallise from host magmas similar to Round Lagoon nephelinite after removal of about 10% olivine, 20–25% diopside, 10–15% nepheline, 5–6% Ti-rich magnetite and 3–4% apatite (Wilkinson & Stolz 1983). These derivatives are limited in volume and are unlikely to deliver phonolitic eruptions at the surface. Furthermore, their mineral compositions are distinct from those in rare phonolites found in Tasmania (Everard *et al.* 2004). In those phonolites, nepheline compositions suggest higher crystallisation T, sodalite lacks a K-component, alkali feldspar includes two types, a Ba-rich and a high K-type, core clinopyroxenes are hedenbergite, amphiboles are arfvedsonite-eckermanite and hastingsite-pargasite, not richterite, and olivine is fayalite. This indicates a different genetic process. The chemical fractionation process within the Round Lagoon nephelinite may include elements of a gas-filter pressure process, where segregation of interstitial liquid takes place after 35–50% crystallisation of the host magma (Rogan *et al.* 1996).

The end fractionate in Round Lagoon nephelinite is a sanidine-diopside-amphibole assemblage, equivalent to alkaline trachyte. The overall late Na-enrichment that developed in the clinopyroxenes relative to Ca, i.e., Na/(Na+Ca) atomic ratio and Mg, i.e., cations per formula unit, ranges from Na/(Na + Ca) 0.63 → 0.91 and Mg 0.46 → 0.13. This follows the evolved pyroxene trend for Teneriffe sodalite-nepheline syenites (Wolff 1987), but at higher Mg levels. It marks an extreme Mg-rich trend (fig. 5) within late-stage alkali pyroxene trends in fractionated alkaline magmas (see Wilkinson 1977, Wolff 1987, Deer *et al.* 1997b, Ridolfi *et al.* 2006). It lies distant from trends related to carbonatitic and more saturated alkaline magma associations.

Mantle xenolith alterations

Early studies on mantle xenolith minerals from undersaturated alkaline lavas found blebs of glassy melts in some assemblages. This led to debates on their origin, whether through a mantle process or a transport decompression process (Scribano 1986, O'Connor *et al.* 1996). In Australian (Victoria) mantle xenolith studies, Yaxley *et al.* (1997) discounted both equilibrium partial melting of peridotite and migration of exotic metasomatic agents for glass generation. They favoured disequilibrium melting of *in situ* metasomatic materials, either through heating or decompressive effects. In a wide study of xenoliths, Coltorti *et al.* (2000) precluded any secondary mineral fractionations as a mechanism for forming the glasses and were able to distinguish glasses derived from mafic melt metasomatism, either sodic or potassic, or carbonatitic metasomatism. Views on whether these glasses formed at mantle depths or by lower pressure decompression during xenolith transport have adherents on both sides. Relatively high-pressure heating, with influx of various metasomatising agents was favoured for melt pockets in xenoliths from a western Hungary basalt field (Bali *et al.* 2008). In contrast, glass compositions and mineral reactions in mantle peridotite were mimicked in melting experiments at one atmosphere with a synthetic alkali host composition (Shaw & Dingwall 2008).

Round Lagoon mantle xenoliths show variable alteration in their mineralogy and textures, particularly through reaction replacements with formation of glassy melt zones. Metawehrlites (pl. 2H) which retain deformation zoned olivine, sieve-texture diopsides and minor Cr-bearing spinel amid extensive recrystallised glassy zones may represent spinel lherzolites, where much orthopyroxene and spinel was reacted and lost constituent elements into the recrystallising melts. The low Al contents and Al co-ordination in the sieved-textured diopsides resemble low-pressure diopside more than the diopside in pristine spinel lherzolite (table 5), suggesting decompression melting at high crustal levels.

Noticeable amounts of reaction products and glassy melt occur within Round Lagoon mantle assemblages compared with some other Tasmanian mantle xenolith suites. This may result from prolonged heating and fluid interaction of the xenoliths during their retention in a relatively slow cooling, fractionating magmatic feeder.

Round Lagoon eruptive reconstruction

The pegmatoids in this plug differ from those formed in ponded surface nephelinite lavas (e.g., at Inverell, La Madera). In the ponded situations, fractionated melts formed during fluxing in cooling horizontal bodies (Wilkinson 1977, Galliski *et al.* 2004). If such lava roofs formed above the Round Lagoon feeder, they have since been eroded away. The Tiers escarpment would be much farther east 25 million years ago, so that former related plateau lavas were possible above this feeder.

Fractionation in the plug operated in a vertical, upward-streaming setting, probably concentrating in favoured zones where enriched flux components (PO_4^{3-}, Cl^{1-}, H_2O, CO_2) inhibited nucleation and increased rates of disequilibrium crystal growth. Rare examples of vertical pegmatoid dykes occur in the plug, but the pegmatoid bodies largely resemble xenoliths in shape and size and may represent fractionation zones disrupted during ongoing magma discharge. The late, less coarse, spherical infilled pegmatoids probably mark residual fractionates that formed in a largely degassed, consolidating magma after final lava discharge.

ACKNOWLEDGEMENTS

D.F. Hendry made valuable additional EMP analyses of the minerals for this study when attached to the Department of Geology and Geophysics, University of Sydney. Facilities for EMP mineral analyses were provided by the Electron Microscope Unit, University of Sydney and the School of Earth Sciences, Macquarie University. The Australian Museum Trust provided funding for the study and the Tasmanian Geological Survey and Mineral Resources Tasmania, Hobart, provided field and laboratory support. The script was read by L.M. Barron, Research Associate, Australian Museum, Sydney. Script preparation was assisted by P. Bayliss, R. Springthorpe, Australian Museum, and F. Kelly, St Peters, Sydney. Constructive reviews of the script were made by P. Carr, School of Earth & Environmental Sciences, University of Wollongong and I. Roach, Department of Earth and Marine Sciences, Australian National University, Canberra. JLE and SMF publish with permission of the Director, Mineral Resources Tasmania.

This paper is dedicated to John F.G. Wilkinson, for his work on low-pressure fractionation of undersaturated alkaline lavas at the University of New England, Armidale, NSW.

REFERENCES

Adam, J. 1990: The geochemisrry and experimental petrology of sodic alkaline basalts from Oatlands, Tasmania. *Journal of Petrology* **31**: 1201–1223.

Adam, J., Oberti, R., Cámara, F. & Green, T.H. 2007: An electron microprobe LAM-ICP-MS and single-crystal X-ray structure refinement study of the effects of pressures, melt-H_2O concentration and $f\,O_2$ on experimentally produced basaltic amphiboles. *European Journal of Mineralogy* **19**: 641–655.

Bali, E., Zanetti, A., Szabó, C., Peate, D.W. & Waight, T.E. 2008: A micro-scale investigation of melt production and extraction in the upper mantle based on silicate melt pockets in ultramafic xenoliths from the Bakony-Balaton Highland volcanic field (Western Hungary). *Contributions to Mineralogy and Petrology* **155**: 165–179.

Briggs, R.M., Rosenberg, M.D., Lange, P.J. de, Itaya, T., King, P.R. & Price, R.C. 1997: Geology and geochemistry of Gannet (Karewa) Island, Tasman Sea: a rift-related nephelinitic tuff ring. *New Zealand Journal of Geology and Geophysics* **40**: 263–273.

Bultitude, R.J. & Green, D.H. 1971: Experimental study of crystal-liquid relationships at high pressures in olivine nephelinite and basanite compositions. *Journal of Petrology* **12**: 121–147.

Cebeira, J.M. 1990: PX: A program for pyroxene classification and calculation. *American Mineralogist* **75**: 1426–1427.

Chazot, G., Menzies, M.A. & Harte, B. 1996: Determination of partition coefficients between apatite, clinopyroxene, amphibole and melt in natural spinel lherzolites from Yemen: implications of wet melting in the lithospheric mantle. *Geochimica et Cosmochimica Acta* **60**: 423–427.

Coltorti, M., Beccaluva, L., Bonadiman, C., Salvini, L. & Siena, F. 2000: Glasses in mantle xenoliths as geochemical indicators of metsomatic agents. *Earth and Planetary Science Letters* **183**: 303–320.

Deer, W.A., Howie, R.A. & Zussman, J. 1982: Olivine. *In Rock-forming Minerals, Volume 1A. Second Edition, Orthosilicates,* Longman, London: 3–336.

Deer, W.A., Howie, R.A. & Zussman, J. 1997a: Diopside-Hedenbergite. *Rock-forming Minerals, Volume 2B, Second Edition, Double-chain Silicates.* The Geological Society, London: 764 pp.

Deer, W.A., Howie, R.A. & Zussman, J. 1997b: Aegirine. *Rock-forming Minerals, Volume 2B, Second Edition, Double-chain Silicates.* The Geological Society, London: 482–519.

Direen, N.G. & Leaman, D.E. 1997: Geophysical modelling of structure and tectonostratigraphic history of the Longford Basin, northern Tasmania. *Exploration Geophysics* **28**: 29–33.

Edgar, A.D. 1984: Chemistry, occurrence and paragenesis of feldspathoids: a review. *In* Brown, W.L. (ed.): *Feldspars and Feldspathoids: Structures, Properties and Occurences.* D. Reidal, Dorrecht, The Netherlands: 501–532.

Eggins, S.M., Rudnick, R.L. & McDonough, W.F. 1998: The composition of peridotites and their minerals: a laser-ablation ICP-Ms study. *Earth and Planetary Sciences Letters* **154**: 53–71.

Everard, J.L. 2001: Inclusions of high pressure origin in Tasmanian Cenozoic basalts: a catalogue of localities. *Tasmanian Geological Survey Record* 2001/09.

Everard, J.L., Sutherland F.L. & Zwingmann, H. 2004: A Cretaceous phonolite dyke from the Tomahawk River, Northeast Tasmania. *Papers and Proceedings of the Royal Society of Tasmania* **138**: 11–33.

Ferguson, A.K. 1977: A note on a ramsayite-bearing pegmatoidal clot in a mela-nephelinite from the Older Volcanics near Bacchus Marsh, Victoria. *Journal of the Geological Society of Australia* **24**: 491–494.

Fodor, R.V., Bauer, G.R. & Keil, K. 1982: Ultramafic inclusions and megacrystals in olivine nephelinite, Aitutaki Island, Cook Islands. *New Zealand Journal of Geology and Geophysics* **25**: 67–76.

Forsyth, S.M. 1989: Geological Survey Explanatory Report. Geological Atlas 1:50 000 Series Sheet 61 (8313 N). Interlaken. *Tasmanian Department of Mines.*

Galliski, M.A., Lira, R. & Dorais, M.J. 2004: Low pressure differentiation of melanephelinitic magma and the origin of ijolitic pegmatites at La Madera, Córboda, Argentina. *Canadian Mineralogist* **42**: 1799–1823.

Green, D.H. & Falloon, T.J. 1998: Pyrolite: A Ringwood concept and its current expression. *In* Jackson, I. (ed.): *The Earth's Mantle. Composition, Structure and Evolution.* Cambridge University Press, Cambridge: 311–378.

Hamilton, D.L. 1961: Nephelines as crystallisation temperature indicators. *Journal of Geology* **69**: 321–329.

Hutchison, C.S. 1974: *Laboratory Handbook of Petrographic Techniques.* John Wiley & Sons, New York: 527 pp.

Johnson, R.W. (ed.) 1989: *Intraplate Volcanism in Eastern Australia and New Zealand.* Cambridge University Press, Cambridge: 408 pp.

Kretz, R. 1983: Symbols for rock-forming minerals. *American Mineralogist* **68**: 277–279.

Leake, B.E. & contributers 1997: Nomenclature of amphiboles: report of the sub-committee on Amphiboles of the International Mineralogical Association, Commission of New Minerals and Mineral Names. *Canadian Mineralogist* **35**: 219–246.

Le Maitre, R.W. (ed.) 2002: *Igneous Rocks: A Classification and Glossary of Terms. Second Edition,* Cambridge University Press, Cambridge: 252 pp.

London, D. 2008: *Pegmatites.* Mineralogical Association of Canada Special Publication 10, Quebec: 368 pp.

McDonough, W.F., McCulloch, M.J. & Sun, S-S. 1985: Isotopic and geochemical systematics in Tertiary-Recent basalts from south eastern Australia and implications for the evaluation of the sub-continental lithosphere. *Geochimica et Cosmochimicia Acta* **49**: 2051–2067.

Mason, D.R. 1985: Polybaric crystallisation of clinopyroxene in ankaramites of the Barrington Tops Tertiary Volcanic Field. *In* Sutherland, F.L., Franklin, B.J. & Waltho, A.E. (eds): *Volcanism in eastern Australia. Geological Society of Australia, New South Wales Division, Special Publication* **1**: 84–105.

Morimoto, N. 1988: Nomenclature of pyroxenes. *Mineralogical Magazine* **52**: 535–550.

O'Connor, T.K., Edgar, A.D. & Lloyd, F.E. 1996: Origin of glass in Quaternary mantle xenoliths from Meerfeldermaar, West Eifel, Germany: implications for enrichment in the lithospheric mantle. *Canadian Mineralogist* **34**: 187–200.

Patic, J.K., Arima, M. & Gupta A.K. 2000: Experimental study of the system diopside-albite-nepheline at P (H_2O) = P(Total) = 2 and 10Kbar and at P(Total) = 28Kbar. *Canadian Mineralogist* **38**: 1177–1191.

Preston, R.J., Hole, M.J. & Still, J. 2000: The occurrences of Zr-bearing amphiboles and their relationships with the pyroxenes and biotites in the teschenite and nepheline syenites of a differentiated dolerite boss, Islay, NW Scotland. *Mineralogical Magazine* **64**: 459–468.

Rawlinson, N., Houseman, G.A., Collins, C.D.N. & Drummond, B.J. 2001: New evidence of Tasmania's tectonic history from a novel seismic experiment. *Geophysical Research Letters* **28**: 3337–3340.

Ridolfi, F., Renzulli, A., Macdonald, R. & Upton, B.G.J. 2006: Peralkaline syenite autoliths from Kilombe volcano, Kenya Rift Valley: Evidence for subvolcanic interaction with carbonatitic fluids. *Lithos* **91**: 373–392.

Rogan, W., Blake, S. & Smith, I. 1996: In situ chemical fractionation in thin basaltic lava flows: examples from the Auckland volcanic field, New Zealand and a general

physical model. *Journal of Volcanology and Geothermal Research* **74**: 89–99.

Scribano, V. 1986: The harzburgite xenoliths in a Quaternary basanitoid lava near Scordia (Hyblean Plateau, Sicily). *Rendictoni Società Italiana di Mineralogia e Petrologia* **41**(2): 245–255.

Shaw, C.S.J. & Dingwell, D.B. 2008: Experimental peridotite-melt reaction at one atmosphere: a textural and chemical study. *Contributions to Mineralogy and Petrology* **155**: 199–214.

Simonetti, A., Shore, M. & Bell, K. 1996: Diopside phenocrysts from nephelinitic lavas, Napak volcano, eastern Uganda: Evidence for magma mixing. *Canadian Mineralogist* **34**: 411–421.

Smith, I.E.M., Blake, S., Wilson, C.J.N. & Houghton, B.F. 2008: Deep seated fractionation during the rise of a small volume basalt magma batch: Crater Hill, Auckland, New Zealand. *Contributions to Mineralogy and Petrology* **155**: 511–527.

Spera, F.J. 1984: Carbon dioxide in petrogenesis: 111. Role of volatiles in the ascent of alkaline magma with special reference to xenolith-bearing mafic lavas. *Contributions to Mineralogy and Petrology* **88**: 217–232.

Sun, S-S. & McDonough, W.F. 1989: Chemical and isotopic systematics of oceanic basalts: implications for mantle composition and processes. *In* Saunders, A.D. & Norry, M.J. (eds): *Magnetism in the Ocean Basins. Geological Society Special Publication* No. **42**: 313–345.

Sutherland, F.L. 1974: High-pressure inclusions in tholeiitic basalt and the range of lherzolite-bearing magmas in the Tasmanian volcanic province. *Earth and Planetary Science Letters* **24**: 317–232.

Sutherland, F.L. 1989: Cainozoic volcanic rocks. *In* Forsyth, S.M. (Compiler): Geological Survey Explanatory Report. Geological Atlas 1:50 000 Series Sheet 61 (8313N). Interlaken. *Tasmanian Department of Mines*: 48–60.

Sutherland. F.L. & Hollis, J.D. 1982: Mantle-lower crust petrology from inclusions in basaltic rocks in eastern Australia – an outline. *Journal of Volcanology and Geothermal Research* **14**: 1–29.

Sutherland F.L. and contributors 1989: Tertiary volcanism, Tertiary basaltic magmas and the Tasmanian lithosphere. *In* Burrett, C.F. & Martin, E.L. (eds): Geology and Mineral Resources of Tasmania. *Geological Society of Australia Special Publication* **15**: 383–398.

Sutherland, F.L., Graham, I.T., Everard, J.L., Forsyth, S.M. & Zwingmann, H. 2004: Cenozoic basalts, Tasmania: Landscapes, exposures, ages, petrology, geochemistry, entrainments and petrogenesis. *Geological Society of Australia* Field Guide A5, Sydney: 58 pp.

Sutherland, F.L., Hendry, D.F., Barron, B.J., Matthews, W.L. & Hollis, J.D. 1996: An unusual Tasmanian Tertiary basalt sequence near Boat Harbour, Northwest Tasmania. *Records of the Australian Museum* **48**: 131–161.

Sutherland, F.L., Raynor, L.R. & Pogson, R.E. 2005: Table Cape xenolithic suite, northwest Tasmania: Mineralogy and implications for crust-mantle lithology and Miocene geotherms in Tasmania. *Papers and Proceedings of the Royal Society of Tasmania* **139**: 7–22.

Ulrych, J., Lloyd, F.E., Balogh, K., Hegner, E., Langrová, A., Lang, M., Novák, J.K. & Řanda, Z. 2005: Petrogenesis of alkali pyroxenite and ijolite xenoliths from the Tertiary Loučná-Oberweisenthal Volcanic Centre, Bohemian Massif in the light of new mineralogical, geochemical, and isotopic data. *Neues Jahrbuch für Mineralogie-Abhandlungen* **182**: 57–59.

Ulrych, J., Pivec, E., Lang, M. & Lloyd, F.E. 2000: Ijolite segregations in melilite nephelinite of Podhorni vrch volcano, Western Bohemia. *Neues Jahrbuch für Mineralogie-Abhandlungen* **175**: 317–348.

Wass, S.Y. 1979: Multiple origins of clinopyroxenes in alkali basaltic rocks. *Lithos* **12**: 115–132.

Wells, P.R.A. 1977: Pyroxene thermometry in simple and complex systems. *Contributions to Mineralogy and Petrology* **62**: 129–130.

Wilkinson, J.F.G. 1977: Petrogenetic aspects of some alkali volcanic rocks. *Journal & Proceedings of the Royal Society of New South Wales* **110**: 117–138.

Wilkinson, J.F.G. & Stolz, A.J. 1983: Low pressure-fractionation of strongly undersaturated alkaline ultrabasic magma: the olivine-melilite-nephelinite at Moiliili, Oahu, Hawaii. *Contributions to Mineralogy and Petrology* **83**: 363–374.

Wittke, J.H. & Holm, R.F. 1996: The association basanitic nephelinite-feldspar ijolite-nepheline monzosyenite at House Mountain volcano, north-central Arizona. *Canadian Mineralogist* **34**: 221–240.

Wolff, J.A. 1987: Crystallisation of nepheline syenite in a subvolcanic magma system: Teneriffe, Canary Islands. *Lithos* **20**: 207–223.

Woodland, A.B. & Jugo, P.J. 2007: A complex magmatic system beneath the Devès volcanic field, Massif Central, France: evidence from clinopyroxene megacrysts. *Contributions to Mineralogy and Petrology* **153**: 719–731.

Yavuz, F. 1996: Amphcal: A quick basic program for determining the amphibole name from electron microprobe analyses using the IMA rules. *Computers and Geosciences* **22**: 101–107.

Yaxley, G.M., Kamenestky, V., Gran, D.H. & Falloon, T.J. 1997. Glasses in mantle xenoliths from western Victoria, Australia and their relevance to mantle processes. *Earth and Planetary Science Letters* **148**: 433–466.

Zhou, J. & Li, X. 2006: GeoPlot: An Excel VBA program for geochemical data plotting. *Computers and Geosciences* **32**: 554–560.

(accepted 7 October 2008)